



**HAL**  
open science

## Highlighting the "Structure-Reactivity" relationship for the autoxidation reaction of hydrocarbons

Soraya Aminane, Mickaël Sicard, Lorette Sicard, Frédéric Ser

► **To cite this version:**

Soraya Aminane, Mickaël Sicard, Lorette Sicard, Frédéric Ser. Highlighting the "Structure-Reactivity" relationship for the autoxidation reaction of hydrocarbons. IASH Symposium-17TH INTERNATIONAL CONFERENCE ON STABILITY, HANDLING AND USE OF LIQUID FUELS, Sep 2022, Dresde, Germany. hal-03842405

**HAL Id: hal-03842405**

**<https://hal.science/hal-03842405v1>**

Submitted on 7 Nov 2022

**HAL** is a multi-disciplinary open access archive for the deposit and dissemination of scientific research documents, whether they are published or not. The documents may come from teaching and research institutions in France or abroad, or from public or private research centers.

L'archive ouverte pluridisciplinaire **HAL**, est destinée au dépôt et à la diffusion de documents scientifiques de niveau recherche, publiés ou non, émanant des établissements d'enseignement et de recherche français ou étrangers, des laboratoires publics ou privés.

*IASH 2022, the 17<sup>TH</sup> INTERNATIONAL CONFERENCE ON STABILITY, HANDLING  
AND USE OF LIQUID FUELS  
Dresden, Germany  
11-15 September 2022*

**HIGHLIGHTING THE "STRUCTURE-REACTIVITY" RELATIONSHIP  
FOR THE AUTOXIDATION REACTION OF HYDROCARBONS**

Soraya Aminane,<sup>1</sup> Mickaël Sicard,<sup>1</sup> Lorette Sicard,<sup>2</sup> Frédéric Ser<sup>1</sup>

<sup>1</sup> DMPE, ONERA Université Paris Saclay, Palaiseau, F-91123, France,  
[soraya.aminane@onera.fr](mailto:soraya.aminane@onera.fr)

<sup>2</sup> Laboratoire ITODYS, 15 Rue Jean Antoine de Baïf, 75013 Paris, France, [lorette.sicard@univ-paris-diderot.fr](mailto:lorette.sicard@univ-paris-diderot.fr)

**ABSTRACT**

The aim of this study was to investigate the mechanisms and kinetics reaction for hydrocarbon molecules composing a jet fuel. Five model hydrocarbons were selected (n-dodecane and its isomers blend, n-butylcyclohexane, 1,2,4-trimethylbenzene and 1-methylnaphthalene) and subjected individually to oxidation using the PetroOXY device, focusing on the beginning of autoxidation ( $\Delta P/P_{\max} = 2$  to 10 %). The consumption of oxygen was always higher than that of the parent hydrocarbons suggesting competitive reactions. Although the oxygen consumption is globally similar for the all alkanes, it is variable for the aromatics. This illustrates their reactivity confirmed by the induction periods (IP). An experimental protocol was developed to identify and quantify precisely the oxidation products formed in the gas and liquid phases, using analytical and chemical techniques. A link between the initial hydrocarbon's structure and the nature and number of carbon atoms in the oxidized products was evidenced. In addition, the tests performed at different temperatures (140, 150 and 160 °C) enabled the calculation of the overall and hydroperoxide dissociation kinetics constants reaction. Arrhenius parameters values obtained were higher for alkanes than for aromatics, confirming the "structure-reactivity" relationship of hydrocarbons.

**Keywords:** PetroOXY, model molecule, structure-reactivity, kinetics constants.

## INTRODUCTION

One concern of the aviation industry is the jet fuel thermal stability. When not guaranteed, it leads to the formation of insoluble deposits in the fuel system and injectors, causing clogging and failures. The deposits is a result of the formation of soluble or insoluble products which can be generated at moderate temperatures, between 140 and 250 °C, by the autoxidation phenomenon. During this process, oxygen naturally dissolved in the jet fuel (70 ppm) interacts with the hydrocarbon molecules through a free radical mechanism. The process is described in the literature as a four-step mechanism: initiation, propagation (in two sub-steps) and termination [1], resulting in the formation of four classes of species: primary oxidation products (hydroperoxides) [2], secondary oxidation products (soluble oxidized products) [3-6], soluble macromolecular oxidation reactive species (SMORS) [7-9] and insoluble deposits [8-12]. It is established that the thermal stability of jet fuel is very dependent on the operating conditions. Many research studies have shown that deposits formation results from the contribution of the thermodynamic conditions in the fuel system (temperature [15], pressure [16-17,20]), time-dependent parameters (residence time [14], flow rate [17]), geometrical and technological characteristics (the nature of the materials [18-19] and the diameter [14,20,21] of the functional element under consideration), as well as the particular operating conditions (transient, steady-state or shutdown phase) [22,23]. Beyond the operating conditions of jet fuel, several studies have shown that the deposits formation depends of the nature of the constitutive hydrocarbon molecules, as well as of interactions with oxygen [10,15,18,24], or trace species such as heteroatomic species [25-29] dissolved metals [18,30-32] and additives [33]. These various parameters are not necessarily independent and their combination can have a significant impact on the formation of deposits, and therefore on the operation of the aircraft.

Although several hypotheses have been proposed to explain the formation of deposits, the exact nature of the precursors and their formation mechanism could not be established. Recent investigations have highlighted the potential polar nature of these species, which may derive from polymerisation reactions [12] of soluble species or the precipitation of SMORS [9,11] or an esterification reaction. [10] Overall, it was found that the nature of the oxidation products in the liquid phase has an impact on the reactivity of the deposits formation mechanism. As jet fuel is a complex blend of chemical compounds, mostly hydrocarbon molecules with different structures, they will have different oxidation reactivities and therefore different oxidation products in terms of nature and quantity.

In a previous paper [6], we studied the oxidation of n-dodecane, using the PetroOXY device, for  $\Delta P/P_{\max} = 0$  to 10 % and  $T = 140$  to 160 °C. Under these conditions, it was possible to identify and quantify the different products resulting from its degradation in the gas and liquid phases. In addition, this study allowed to determine the mechanisms and the kinetic constants of degradation for linear alkanes. The aim of the present work is to examine the degradation mechanisms and kinetics of the hydrocarbons composing Jet A-1 with the same methodology to better understand their chemical structure impact in the formation of oxidative deposition


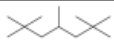
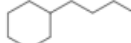
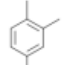
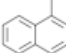
precursors. Considering the complexity of the interactions and the contribution of minor species to the formation of deposits, five model hydrocarbons were selected: n-dodecane and its isomers blend, n-butylcyclohexane, 1,2,4-trimethylbenzene and 1-methylnaphthalene. These molecules were individually subjected to oxidation using the PetroOXY device, focusing on the onset of autoxidation ( $\Delta P/P_{\max} = 2 - 10 \%$ ) at a temperature and initial dioxygen pressure of 160 °C and 700 kPa, respectively.

## EXPERIMENTAL SECTION

### Materials

Hydrocarbons belonging to five families of hydrocarbons (linear and branched alkanes, cycloalkanes, mono and diaromatics) were selected. Their characteristics are presented in Table 1.

*Table 1 - Properties of the selected hydrocarbon molecules*

Model compounds	Abbreviations	Molar weight (g.mol <sup>-1</sup> )	Purity (%)	Formula
n-dodecane C <sub>12</sub> H <sub>26</sub>	n-C <sub>12</sub>	170,34	99	
n-dodecane isomers blend C <sub>12</sub> H <sub>26</sub>	n-C <sub>12</sub> IsoB	170,34	95	
n-butylcyclohexane C <sub>10</sub> H <sub>20</sub>	n-BC	140,27	99	
1,2,4-trimethylbenzene C <sub>9</sub> H <sub>12</sub>	1,2,4-TMB	120,19	98	
1-methylnaphthalene C <sub>11</sub> H <sub>10</sub>	1-MN	142,20	96	

### Method

#### *PetroOXY device*

The PetroOXY device (Anton Paar) was used to study the stability towards oxidation of the fuels. [34] 5 mL of hydrocarbon is poured into a glass crucible. In order to assure that oxygen is the only dissolved gas; the fuel is degassed 2 min in an ultrasonic bath. The crucible is then introduced into a chamber hermetically closed. In order to obtain sufficient deposits, the tests were carried out at  $\Delta P/P_{\max} = 10 \%$  at an initial static oxygen pressure set at 700 kPa and at an initial temperature of 160 °C. These physical features are continuously measured during the experiment. All the samples are tested 4 times to verify the repeatability and to have enough oxidized liquid to characterize. After the test, the gas and liquid phases are recovered after cooling down the device down to 25 °C.

## **Characterization techniques**

### ***Micro-Gas Chromatography***

The gas phase was also analyzed by micro-GC (Agilent 490). The apparatus is equipped with Thermal Conductivity Detectors (TCD) and 3 columns: Al<sub>2</sub>O<sub>3</sub> (10 m × 0.32 ID, T<sub>column</sub> = 70 °C, P = 130 kPa), CO<sub>x</sub> (1 m × 0.7 ID, T<sub>column</sub> = 80 °C, P = 150 kPa), CP sil-5CB (20 m, T<sub>column</sub> = 50 °C, P = 150 kPa). The analysis was carried out with helium and argon as vector gas. Calibration was made before each test for H<sub>2</sub>, CO, CO<sub>2</sub>, and the hydrocarbon molecules.

### ***Gas Chromatography-Mass Spectrometry***

The liquid phase was analyzed by Gas Chromatography coupled to a mass spectrometer (GC-MS) with a Varian 450 GC/320 MS. This apparatus is equipped with an automatic sampler CP-8410, an injector 1177 split/splitless, a capillary column PONA type, a fused silica capillary column (phase type: VF-5 ms, length: 60 m, internal diameter: 0.25 mm, phase thickness: 1 μm) with a column flow of 0.8 mL/min and a Flame Ionization Detector (FID). The analysis was carried out with helium as the vector gas. The injection temperature was set at 250 °C. The thermal program was optimized for all molecules: 5 min at 50 °C; heating up to 175 °C (at a speed of 5 °C.min<sup>-1</sup>) for 5 min then to 250 °C (10 °C. min<sup>-1</sup>) for 45 min. Standards were prepared by mixing different volumes of hydrocarbons and *n*-decane (purity > 99 %, Alfa Aesar) for alkanes and *n*-dodecane for aromatics model molecules. These standard solutions and the oxidized samples were injected 3 times and a deviation of less than 1 % was imposed. The MS fragmentation was obtained by an electronic impact of 70 eV.

### ***Steric Exclusion Chromatography***

Liquid phase analysis was supplemented by SEC using tetrahydrofuran (THF, 99.9 %, Acros Organics) for elution. The Perkin Elmer 200 chromatograph was equipped with an automatic sampler with an injection loop of 200 μL, two analytical columns (30 cm) for detection by both differential refractometry (IOTA2 detector) and UV absorption (diode array detection) at 250 nm. The samples were prepared by adding 500 μL of THF to 50 μL of oxidized hydrocarbon.

### ***High Performance Liquid Chromatography***

High Performance Liquid Chromatography (HPLC) for qualitative analysis of the liquid phase, was carried out with a Prostar/Prepstar 218, from Varian, using an automatic sampler (ProStar 410) and a UV detector (ProStar 335, λ = 230 nm). Separation was obtained with an apolar column (2.6 μm-sized silica particles grafted by octadecyl chains, porosity 100 Å) using a water / acetonitrile (> 99.7 %, Alfa Aesar). eluent (30 to 100 %). The samples were prepared by adding 500 μL of ACN to 100 μL of the solution to be analyzed. 5 μL of the resulting mixture were injected.

## **Quantification of the products formed**

### ***Identification of hydroperoxide species***

The presence of hydroperoxide species was evidenced through the oxidation of triphenylphosphine (TPP) to the corresponding oxide (TPPO) [35,36] according to the reaction :  $ROOH + TPP \rightarrow TPPO + ROH$ .

For this purpose, 4 g of TPP (99 %, Acros Organics) and 0.3 g of fluorene (> 98 %, Acros Organics) were dissolved in 50 mL of chloroform ( $\geq 99.8$  %, Carl Roth). 250  $\mu$ L of this solution were added to 1 mL of oxidized model molecules and stirred for 10 min before analysis by GC and GC-MS. The limit of detection of this method is less than 0.002 mM.

### ***Peroxide Value (PV)***

Peroxide species formed during the test were back titrated using a method close to that described in the ASTM D3703[37], relying on the reduction of the iodide molecules formed during titration with sodium thiosulfate. The Peroxide Value (PV) was calculated according to Equation 1, where A and B are the volumes of a sodium thiosulfate solution, of normality N, added during the assay and a blank test, respectively, to a volume V of sample.[36]

$$PV = \frac{((A - B) N \times 1000)}{V} \quad \text{Equation 1}$$

### ***Total Acid Number (TAN)***

The total acid number (TAN) is the mass of KOH needed to neutralize the free acid molecules present in 1 g of sample [38]. The method employed to determine the TAN is based on the ASTM D3242 [39]. It is an acido-basic titration, suitable in the range from 0.00 to 0.10 mg KOH/g.

### ***Water Content***

The water content was determined by coulometric titration with a Karl-Fisher titrator (Mettler Toledo C30 with a Pt electrode under 20  $\mu$ A). The anolyte and catolyte used were the HYDRANAL Coulomat AK and HYDRANAL Coulomat CGK solutions Honeywell Fluka, respectively.

## **RESULT AND DISCUSSION**

### **Consumption of reagents**

The selected molecules (Table 1) were oxidized with the PetroOXY device at a temperature and an initial pressure of 160 °C and 700 kPa, respectively, and then stopped at low  $\Delta P/P_{max}$  values: 2, 4, 6, 8 and 10 %, in order to study the beginning of the autoxidation process. Figure 1.a) shows the evolution of the pressure with reaction duration for all the model molecules. Except for 1-MN, for which test durations are very long (3 to 10 h between  $\Delta P/P_{max} = 2$  and 10 %, respectively), for the other oxidized model molecules the test duration are short and vary from 20 to 40 min, for 2 to 10 %. This suggests that, among the selected model molecules, diaromatic molecules show a better oxidation stability. However, as shown on Figure 1.b), the induction period of the tests follows a linear evolution no matter what the oxidized molecule is. This result

indicates that the rate of O<sub>2</sub> consumption is constant in the range the  $\Delta P/P_{\max}$  (2 to 10 %) for all the molecules.

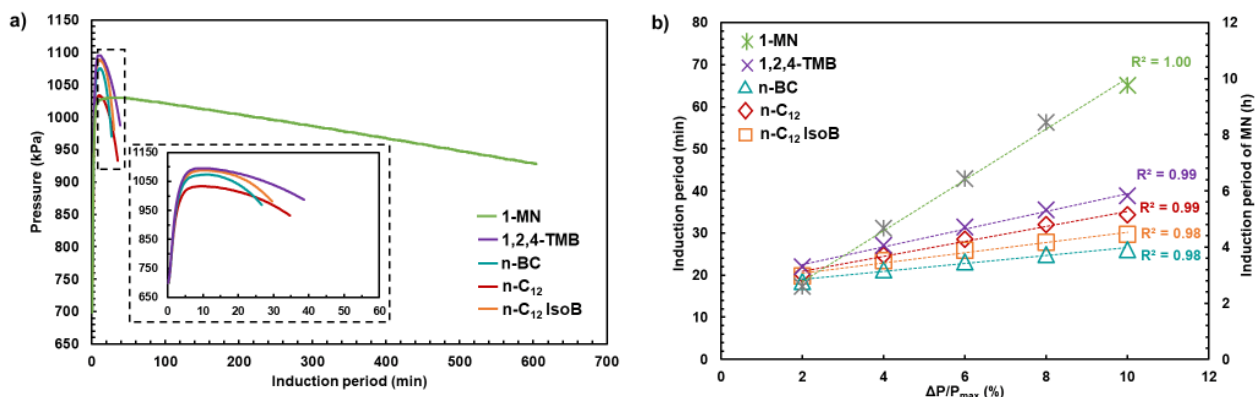


Figure 1 - Evolution of the oxidation of model molecules at 160 °C and  $P_{O_2,i} = 700$  kPa with a) pressure versus duration time at  $\Delta P/P_{\max} = 10$  % and b) induction period versus  $\Delta P/P_{\max}$

The number of moles of O<sub>2</sub> and of hydrocarbon model molecules consumed was followed for the tests duration as shown in Figure 2. It is expected that these two figures should be equal as 1 O<sub>2</sub> should react with 1 hydrocarbon molecule but the consumption of O<sub>2</sub> was much higher for all the molecules except 1,2,4-TMB. Indeed, at  $\Delta P/P_{\max} = 10$  %, the molar ratios of O<sub>2</sub>/parent molecule are 5:1, 7.8:1, 4.3:1 and 8.2:1 for the n-C<sub>12</sub>, n-C<sub>12</sub> IsoB, n-BC and 1-MN, respectively. This suggests that the oxygen reacts, on the one hand, with the hydrocarbon molecule present at the initial state and, on the other hand, with the oxidation products. In contrast, in the case of the oxidation of 1,2,4-TMB (Figure 2.d.), the reagent consumptions (O<sub>2</sub> and 1,2,4-TMB) are very close: the molar ratio O<sub>2</sub>/1,2,4-TMB consumed is 1.4:1.

Overall, the results in Figure 2 indicate that the consumption of the reagents follows a linear evolution and increases with the reaction progress. This confirms the Figure 1.b. observations, according to which the consumption rate of O<sub>2</sub> is constant whatever the nature of the oxidized molecule. This figure also shows that the number of moles of O<sub>2</sub> consumption decreases in the following order: Branched alkanes >> Alkanes >> Aromatics. This is noteworthy as it demonstrates a different behavior according to the chemical structure of the oxidized molecules, linked to the sensitivity of the hydrocarbons to oxidation, as illustrated by the induction times (Figure 1).

Concerning the model hydrocarbon molecules, their consumption is very low (< 0.0012 moles of hydrocarbon consumed) and depends on the nature of the oxidized molecule in the following order: Mono-aromatic >> Alkanes > Di-aromatic.

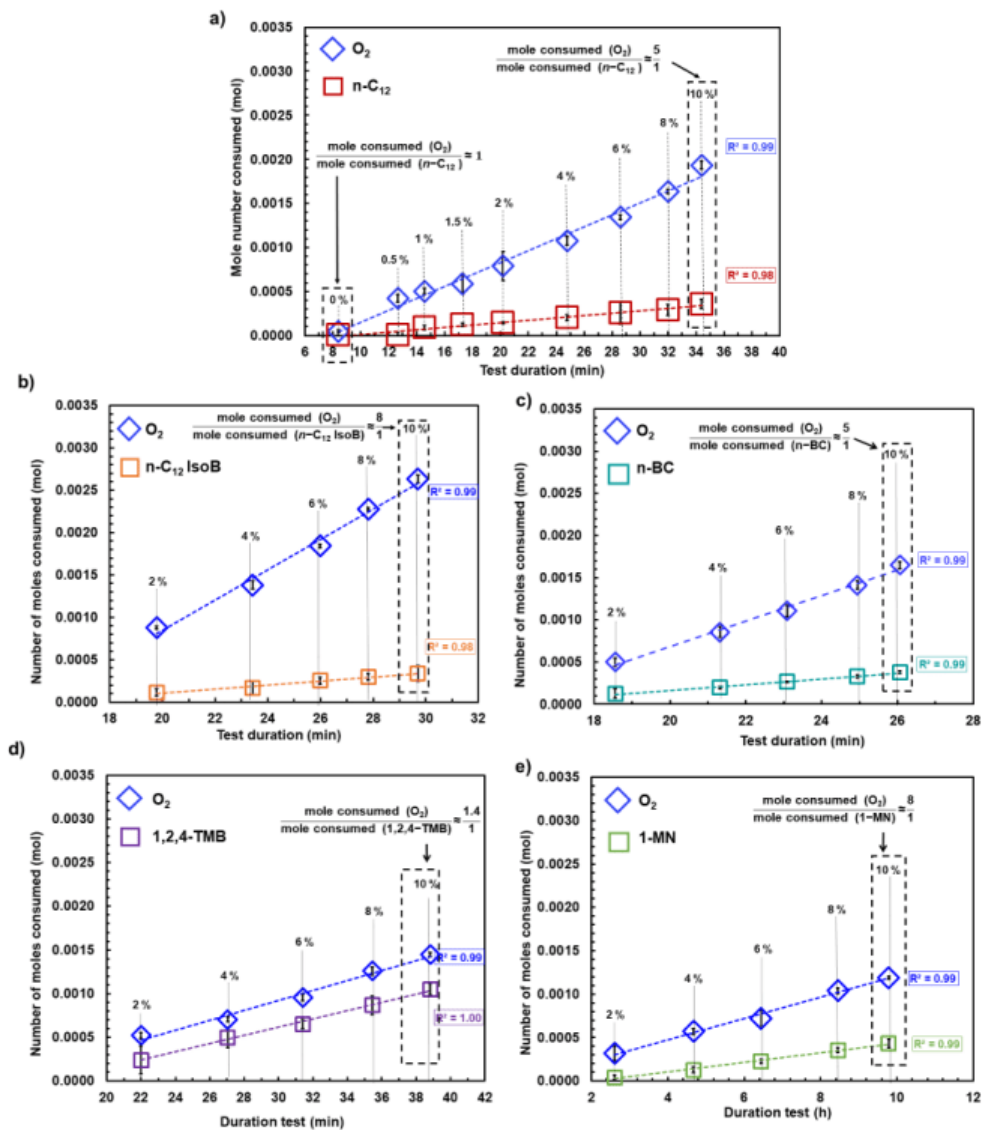


Figure 2 – Mole number consumed of  $O_2$  and model molecules, with a)  $n-C_{12}$ , b)  $n-C_{12}$  IsoB, c)  $n-BC$ , d) 1,2,4-TMB and e) 1-MN, as a function of the induction period during their oxidation ( $T = 160\text{ }^\circ\text{C}$ ,  $P_{O_2,i} = 700\text{ kPa}$ )

## Gas phase analysis

The analysis of the gas phase was performed by micro-GC to identify specifically the molecules formed.  $H_2$ ,  $CO_2$ ,  $CO$ ,  $CH_4$ , alkanes and alkenes ranging from  $C_2$  to  $C_5$ , as well as polar molecules such as water, formaldehyde, alcohols (methanol, ethanol, propanol), and acetone were identified. All these molecules begin to form at an early stage,  $\Delta P/P_{\max} = 2\%$ , however they are detected significantly later, at  $\Delta P/P_{\max} = 10\%$ .

The volume of gas species was quantified. Figure 3 shows the volume percentage gas results converted to ppm concentration. In Figure 3.a. are presented the amounts of  $CO_2$ ,  $H_2$  and  $CO$  and in Figure 3.b. the amounts of  $CH_4$ , alkanes and alkenes, obtained at  $P/P_{\max} = 10\%$  and a fixed temperature and pressure of  $160\text{ }^\circ\text{C}$  and  $700\text{ kPa}$ . The volume of gas formed is very low for all



the oxidized model molecules ( $< 60000$  ppm of gas by volume or 0.06 %).  $\text{CO}_2$  is the gas formed in majority whatever the oxidized molecule (Figure 3.a) is. The other identified gases which follow in decreasing quantity are:  $\text{H}_2$ ,  $\text{CO}$ ,  $\text{CH}_4$ , the alkenes and then alkanes. Furthermore, it is noteworthy that the amounts of gas formed depend on the nature of the molecule and its chemical structure. Indeed,  $\text{CO}_2$  is formed in increasing amount when oxidizing  $1,2,4\text{-TMB} < n\text{-BC} < n\text{-C}_{12} < 1\text{-MN} < n\text{-C}_{12}$  IsoB (Figure 3.a.). Thus, the branched alkane molecule gives more  $\text{CO}_2$  than the mono aromatic molecule (40 times more). Moreover, the amount of  $\text{CO}_2$  formed for 1-MN is, at least, 2 times higher than that of  $n\text{-C}_{12}$  and  $n\text{-BC}$ . This indicates a different oxidation reactivity based on the chemical structure of the oxidized molecule.

The results presented in Figure 3.b. confirm this hypothesis. Indeed, a much higher amount of  $\text{CH}_4$  is formed for aromatic (mono- and di-) than for alkane molecules (linear, branched and cyclic). In contrast, in the case of alkenes, the opposite trend is observed. Thus, aromatic molecules will tend to form more  $\text{CH}_4$  and alkane molecules preferentially alkenes.

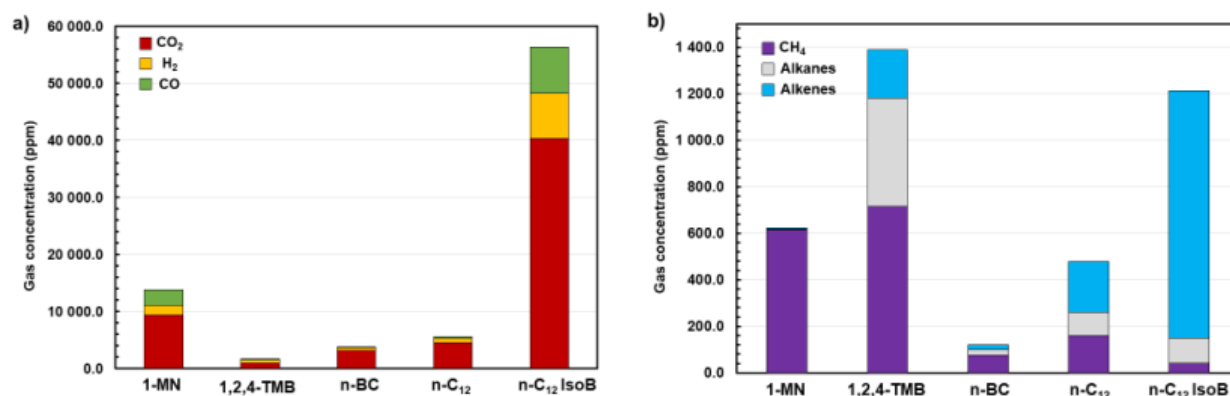


Figure 3 - Comparison of the gas quantity formed during the oxidation of the model molecules, determined from the quantitative analysis by micro-GC ( $\Delta P/P_{max} = 10\%$ ,  $T = 160\text{ }^\circ\text{C}$ ,  $P_{O_2,i} = 700\text{ kPa}$ )

The molecule that forms the most significant amount of total gas is  $n\text{-C}_{12}$  IsoB. This implies a specific reactivity for the branched alkane structure. Beyond the quantitative aspect of the molecules formed, this analysis highlights the "structure-reactivity" aspect, illustrated in particular by the influence of the branching of the initial hydrocarbons. The more branches a molecule is, the more carbon chain breaking reactions can take place. This can be illustrated during the oxidation of the branched alkane, which structure allows mechanisms corresponding to a significant break in the chain, highlighted by a high quantity of gas, involving a large quantity of light molecules. In contrast, the lowest amount of total gas formed is observed for the oxidation of 1,2,4-TMB. This can be explained by the mono aromatic structure and the short length of the branches.

### Liquid phase analysis

The liquid phase was first analyzed by SEC and HPLC obtained with an UV detector (Figure 4.a. and b.), respectively. In the case of di- and mono-aromatic molecule, shoulders can be seen in

Figure 4.a after degradation before the main peaks at 16.5 and 15.5 min corresponding to 1-MN and 1,2,4-TMB, respectively. This accounts for the presence of molecules of higher and equal sizes than the initial molecules. These results are further confirmed on the HPLC chromatograms (Figure 4.b.) displaying several peaks showing the formation of polar molecules. By correlating the SEC and HPLC results (Figure 4), it is possible to deduce the formation of oxidized molecules, with chain length equal to that of the 1-MN in the case of the oxidation of a molecule with a di-aromatic structure and with size higher than or equal to that of the 1,2,4-TMB in the case of the molecule with a mono-aromatic structure.

In the case of the alkane molecules, a strong peak corresponding to the initial non-oxidized molecules is observed on the SEC chromatograms at 14.5 min for n-BC and at 13.5 min for n-C<sub>12</sub> and n-C<sub>12</sub> IsoB. Additional peaks are observed after oxidation at retention times lower and higher than those of the main peaks, suggesting the formation of additional molecules with dimensions smaller and larger than the initial molecule.

In contrast, in the case of linear and branched alkanes (n-C<sub>12</sub> and n-C<sub>12</sub> IsoB), the molecules formed have a chain length essentially shorter or equal to the initial molecule. These observations are correlated to the HPLC results (Figure 4.b.) which confirm the size of the molecules formed and inform us about the polar nature of the products formed.

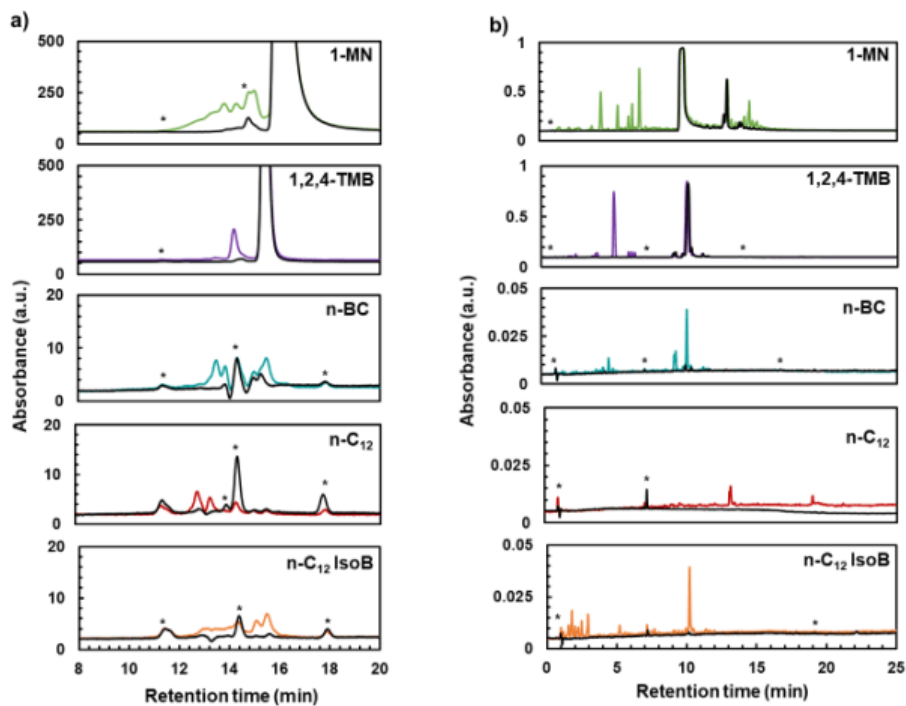


Figure 4 - Chromatograms obtained with UV detectors by a) SEC, b) HPLC) of the liquid phase of the initial model molecules (black curves) and after their oxidation at  $\Delta P/P_{max} = 10\%$  ( $T = 160\text{ }^{\circ}\text{C}$ ,  $P_{O_2,i} = 700\text{ kPa}$ ) with (\*) THF and ACN impurities depending on the technique used (SEC and HPLC, respectively)

The liquid phase analysis was supplemented by GC-MS to characterize the oxidation products (Figure 5 and 6). The products generated during the oxidation process are identical for all

oxidized model molecules. Furthermore, the retention peaks are identical, regardless of the progress of the reaction, and their intensities increase with time. This implies that the same products are formed during the whole oxidation process and that their quantity increases with the duration of the reaction, involving the same reaction mechanisms. In addition, no accumulation of any particular molecule is observed. The peaks corresponding to the non-oxidized model molecules (1-MN, 1,2,4-TMB, n-BC, n-C<sub>12</sub> and n-C<sub>12</sub> IsoB) are located at 40, 25, 28, 34 and 27 min of retention time respectively.

The chromatograms obtained for the di- and mono-aromatic molecules (1-MN and 1,2,4-TMB) are shown in Figure 5.a. and b. respectively. For these molecules, very few compounds are formed for retention times lower than the model molecule. This important result suggests that the oxidation products have a molecular mass equivalent or higher than the main molecule, thus confirming the results obtained by SEC (Figure 4.a.). From a qualitative point of view, these molecules are alcohols, aldehydes and carboxylic acids (Figure 5.a.2. for 1-MN and Figure 5.b.2. for 1,2,4-TMB). No ketone molecule is detected. The identification obtained by GC-MS of the molecules formed and the analysis of the mass ratios ( $m/z$ ) allowed a better understanding of these results. Indeed, in the case of the aromatic molecules, the alcohol molecules identified are all primary alcohols ( $m/z$  31).

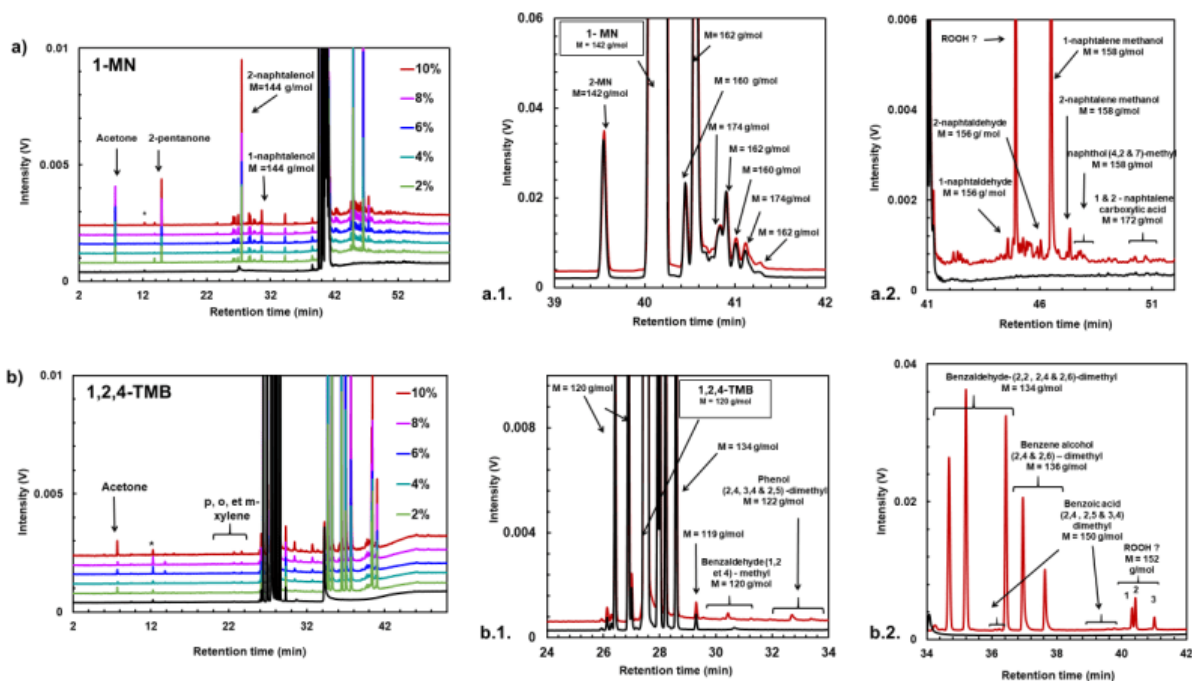


Figure 5 - Chromatograms obtained by GC-MS, of the liquid phase before and after the oxidation of the aromatic molecules at different progress, with (\*) THF impurities ( $T = 160\text{ }^{\circ}\text{C}$ ,  $P_{O_2,i} = 700\text{ kPa}$ ,  $\Delta P/P_{max} = 2-10\%$ ) The figures on the right side show different retention time domains of the chromatograms with unoxidized molecules in black and oxidized molecules at  $\Delta P/P_{max} = 10\%$  in red.

For alkane molecules oxidation (Figure 6), several classes of compounds with different chain lengths are detected. Indeed, for retention times lower than the retention times of the initial molecules of interest, the detected compounds have shorter chain lengths. For the 3 alkane

molecules (n-BC, n-C<sub>12</sub> and n-C<sub>12</sub> IsoB), three types of compounds, namely the carboxylic acid, the 2-ketone and the corresponding aldehyde, with an identical number of carbon atoms are produced. These data confirm the HPLC (Figure 4.b.) results regarding the presence of oxidized products.

Moreover, the formation of oxidized molecules of equivalent or greater size than the initially oxidized molecule is observed for retention times higher than that of the model molecule. For alkane molecules, the oxidation products identified with such chain length are alcohols, ketones, aldehydes and carboxylic acids. The GC-MS mass ratios (m/z) indicate the presence of primary (m/z 31), secondary (m/z 45 and 59) and tertiary alcohols (m/z 87) for cyclic alkanes (n-BC).

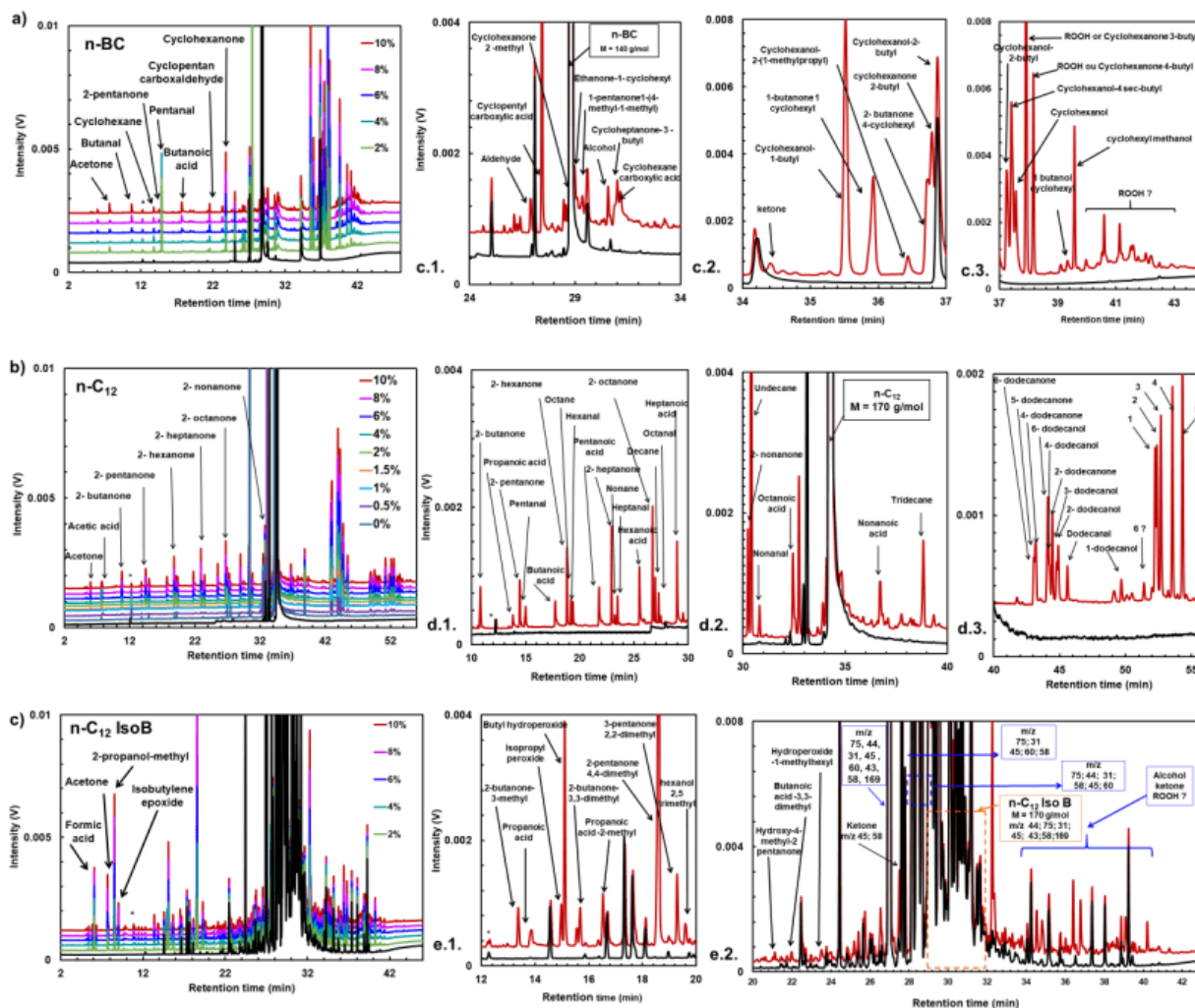


Figure 6 - Chromatograms obtained by GC-MS, of the liquid phase before and after the oxidation of the alkane molecules at different progress, with (\*) THF impurities ( $T = 160\text{ }^{\circ}\text{C}$ ,  $P_{O_2,i} = 700\text{ kPa}$ ,  $\Delta P/P_{max} = 2-10\%$ ) The figures on the right side show different retention time domains of the chromatograms with unoxidized molecules in black and oxidized molecules at  $\Delta P/P_{max} = 10\%$  in red.

With regard to the additional peaks observed for high retention times (above 40 min), GC-MS analysis has revealed the presence of fragments with m/z ratios that can be attributed to hydroperoxide species  $[M - \bullet\text{OOH}]^+$  [40]. In the case of the aromatic molecules, there is one for

1-MN and three for 1,2,4-TMB. In the case of alkane molecules, there are 8 for n-BC and 6 for n-C<sub>12</sub>.

In order to confirm the presence of hydroperoxides, an indirect assay based on their reduction to alcohols in the presence of TriPhenylPhosphine (TPP) was carried out. Thus, if the peaks present on the Figure 5 and 6 correspond to hydroperoxides, the intensity of the alcohols in Figure 7 should increase as the TPP is oxidized into TriPhenylPhosphine Oxide (TPPO). This is exactly what is observed, confirming the attribution of the peaks to the hydroperoxides of the oxidized model molecules. The attribution of hydroperoxides is consequently associated with the number of peaks highlighted in Figure 8. In the case of aromatic molecules, there are one peak for 1-MN and three peaks for 1,2,4-TMB. In view of these observations and considering the initial chemical structure of these molecules, it is possible, in the case of aromatics, to correlate the number of peaks attributed to hydroperoxides to the number of branched methyl groups in the molecule.

Concerning alkane molecules, the number of branches and the structure of the molecules has also an impact on the number of peaks associated with the hydroperoxides isomers. Indeed, in the case of n-BC, 8 peaks are observed, thus revealing the presence of 8 X-butyl cyclohexane hydroperoxides and 6 peaks are observed for n-C<sub>12</sub>, associated with the 6 X-dodecyl-hydroperoxide formed. For the branched alkane molecule (n-C<sub>12</sub> IsoB), the complexity of the isomeric mixture did not allow an exhaustive attribution for the hydroperoxides formed. However, GC-MS analysis reveals the presence of several fragments characteristic of primary alcohols (m/z 31) (Figure 6.c.). In addition, the oxidation of hydroperoxides by TPP, exacerbated peaks present in this region (Figure 7) which can therefore be attributed to alcohols. All these elements support the presence of several hydroperoxides, which could not be detected due to a co-elution phenomenon.

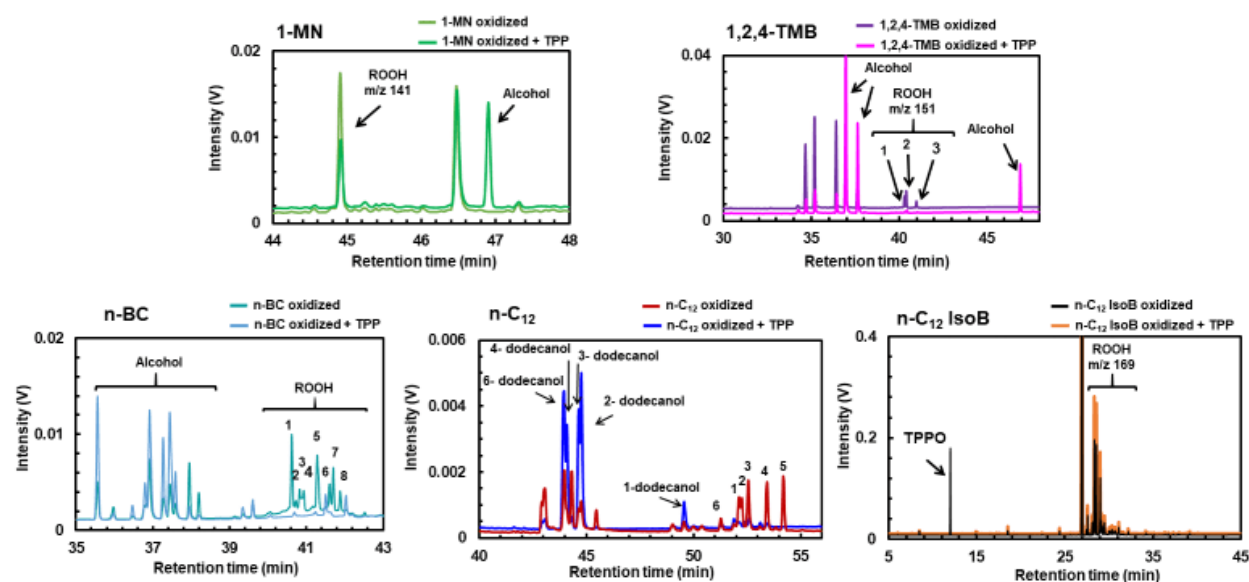


Figure 7 - Comparison of liquid phase chromatograms obtained by GC-MS after oxidation of model molecules at  $\Delta P/P_{max} = 10\%$  without and after addition of TPP ( $T = 160\text{ }^{\circ}\text{C}$ ,  $P_{O_2,i} = 700\text{ kPa}$ )

### **Structure-reactivity aspect**

For all oxidized model molecules, hydroperoxides species are always formed. The secondary oxidation products vary according to the structure of the initial molecule, whether it is linear, branched, cyclic or aromatic. The results of this work have shown that, in the case of alkane molecules, the oxidized products formed are primary and secondary alcohols, ketones, aldehydes and carboxylic acids. For aromatic molecules, the same is true with the exception of secondary alcohols and ketones that are not formed.

Taking into account the products formed and based on the results of SEC, HPLC and GC-MS (Figure 4 to Figure 6), it is possible to divide them into different classes according to the initial structure of the model molecules. In the case of aromatic molecules, we distinguish them into two classes of molecules: hydroperoxides and oxidized products with a carbon chain equal to the initial molecule. In the case of alkane molecules, a third class of oxidation products is distinguished: products with a shorter carbon chain.

#### *The hydroperoxides*

Based on the experimental results, it was possible to establish that, for a given hydrocarbon molecule, the available H atoms induce a number of possibilities of O<sub>2</sub> attacks to form a peroxide radical followed by the formation of a hydroperoxide. This has been demonstrated in particular in the case of the oxidation of aromatic molecules, where TPP results (Figure 7) have shown a direct correlation between the number of methyl groups present in the initial molecule and the hydroperoxides formed. Similarly, for alkane molecules, the number of H atoms in the carbon chain can also be used to deduce the number of hydroperoxides formed, providing that symmetry elements attributed to the chemical structure of these molecules are taken into account.

#### *Oxidized products with carbon chain length equal to the initial hydrocarbon molecule*

Depending on the nature of the attacked carbon, the ROOH species formed will lead to the formation of a primary, secondary or tertiary alcohol. When a primary alcohol is formed (attack of the hydrogen at the end of the chain), the decomposition of the hydroperoxide will lead to a primary alcohol, an aldehyde and then a carboxylic acid. When a secondary alcohol is formed, it oxidizes to a ketone. The mechanisms of formation of these oxidation products have been specifically detailed in a previous paper [6]. Moreover, the oxidation products formed will have a chain length with a number of carbon atoms equal to the chain length of the initial model molecule. Thus for 1-MN and 1,2,4-TMB molecules only primary alcohols can be formed.

For alkane molecules, namely for n-BC and n-C<sub>12</sub> which have a chemical structure able to have a ROOH function on a primary and secondary carbon, then the oxidation products will be a combination of primary and secondary alcohols, ketones, aldehydes and carboxylic acids.

In the case of the branched alkane molecule (n-C<sub>12</sub> IsoB), it was difficult to determine the nature of the molecules formed by GC-MS due to a co-elution phenomenon. It was not possible to specifically identify the oxidation products. However, taking into account the "structure-reactivity relationship" highlighted in this study, as well as the chemical structure of n-C<sub>12</sub> IsoB, as presented in Figure 8, it should be possible to identify 6 hydroperoxide isomers, including:

- 4 will lead to the formation of a primary alcohol, then an aldehyde and a carboxylic acid;
- 1 will lead to a secondary alcohol and then to a ketone;
- 1 will lead to a tertiary alcohol.

Following this reasoning and given the nature of the branching of the aromatic molecules tested, it is not surprising that ketone-type products were not identified because there are no secondary carbons. It would therefore be interesting to carry out a more in-depth study of the structure of the aromatic molecules in order to confirm the impact of branching on the oxidation products formed.

*Oxidized products with carbon chain length less than the initial hydrocarbon molecule:*

In the case of alkane molecules (linear, branched or cyclic), oxidized compounds with shorter chain lengths than the initial alkane molecule are formed. The experimental results (Figure 5 to 6) show the presence of 2-ketones, aldehydes and carboxylic acids with chain lengths shorter than the initial alkane molecule.

It is important to note that their formation does not lead to the production of alcohols. These short-chain oxidized molecules are the result of another type of mechanism, resulting from the formation of a ketohydroperoxide (KPH) [3] and then successive carbon chain breaking reactions. These Korcek reactions are also observed in the case of oxidation reactions at temperatures below 475 °C [41]. It should be noted that the reaction is also an interesting alternative to explain the formation of short carboxylic acids and aldehydes or ketones [3]. These mechanisms have been demonstrated in a previous study on n-C<sub>12</sub> [6]. In contrast, for mono- and di-aromatic molecules, the stability of the benzene rings precludes the possibility of a ring-opening mechanism. This was illustrated earlier by the small amount of gas obtained (Figure 3).

The "structure-reactivity" aspect is illustrated in this study by the influence of the branching of the initial hydrocarbons on the size of the oxidized molecules formed. The more branches a molecule has, the more carbon chain breaking reactions can take place. This was highlighted during the oxidation of the branched alkane (n-C<sub>12</sub> IsoB).

The influence of branching is also confirmed during the oxidation of aromatic molecules, which form secondary oxidation products to a greater or lesser extent depending on the branches that are substituted for the benzene rings of these molecules. Typically, the only oxidation products formed are from the hydrogen atom of the methyl groups.



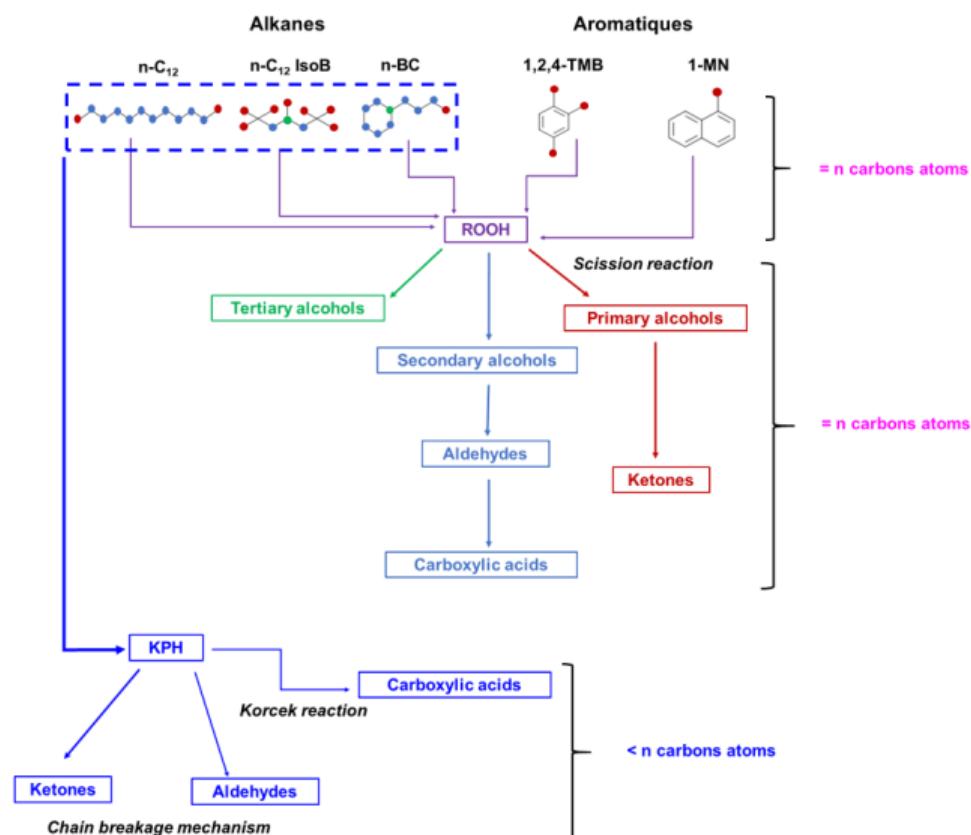


Figure 8 - Global diagram illustrating the different classes of oxidation products obtained for all model molecules with ● primary, ● secondary and ● tertiary carbon

Beyond the nature of the products formed, it was possible to carry out a quantitative analysis of the secondary oxidation products. Different chemical assays were performed: the peroxide value (PV), the total acid number (TAN), related to the amount of carboxylic acids formed, and the water content. All these data are shown in Figure 9.

For the peroxide value (Figure 9.a.), with the exception of n-BC and n-C<sub>12</sub> IsoB which show a logarithmic evolution, for the other molecules a linear and significant increase between  $\Delta P/P_{\max} = 2$  to 10 % was observed. However, it should be noted that the PV varies according to the nature of the oxidized model molecule. Indeed, the amount of hydroperoxide formed follows the following order: 1-MN < n-C<sub>12</sub> IsoB < n-C<sub>12</sub> ~ n-BC < 1,2,4-TMB. The fact that the monoaromatic molecule produces more ROOH than a diaromatic molecule or even an alkane, underlines the fact that the chemical structure of a molecule has an impact on its reactivity to form ROOH.

TAN results (Figure 9.b.) confirm an increasing amount of acid with the reaction progress. Except 1,2,4-TMB which shows an exponential evolution, all the other model molecules display a linear evolution of the TAN between  $\Delta P/P_{\max} = 2$  to 10 %. Moreover, the molecule that forms the most carboxylic acids is n-C<sub>12</sub> IsoB (~ 6 mg KOH/g at  $\Delta P/P_{\max} = 10$  %) while the other molecules form almost 2 times less acids (TAN < 2.5 mg KOH/g). According to Figure 9.b., the TAN values follow the following order: 1,2,4-TMB < 1-MN < n-BC < n-C<sub>12</sub> << n-C<sub>12</sub> IsoB. It



can be concluded that a species with a chemical structure with significant branching favors the formation of carboxylic acids.

Regarding the water quantity produced, it increases significantly for all the oxidized molecules following a linear evolution, except for BC for which evolution is logarithmic. Furthermore, the molecule that forms the most H<sub>2</sub>O quantity between  $\Delta P/P_{\max} = 2$  and 10 % is the 1,2,4 -TMB (508 to 1780 ppm). For the other molecules, the water content is always lower than 500 ppm and the amount formed varies according to the structure of the oxidized molecule in the following order: n-C<sub>12</sub> IsoB < n-BC < 1-MN < n-C<sub>12</sub> << 1,2,4-TMB.

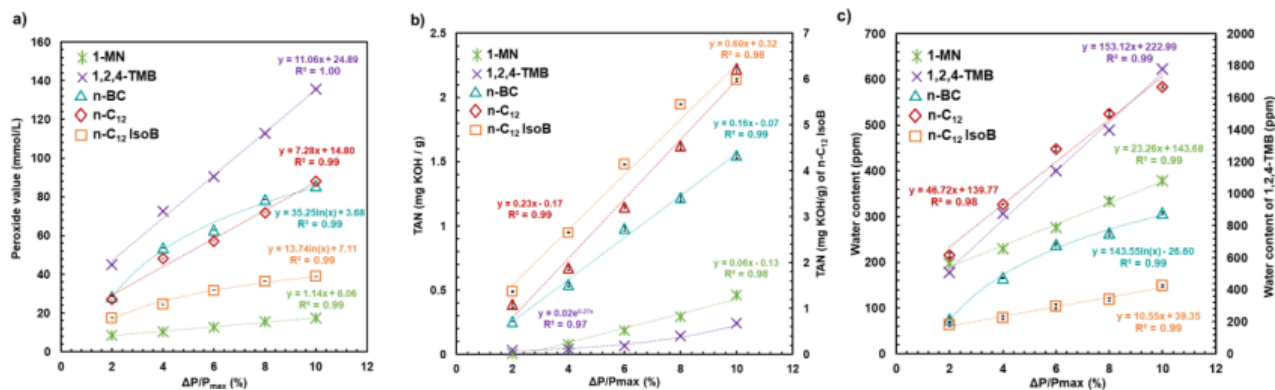


Figure 9 - Evolution of a) PV , b) TAN and c) water content, formed in the liquid phase resulting from the oxidation of the model molecules at different  $\Delta P/P_{\max}$  ( $T = 160$  °C,  $P_{O_2,i} = 700$  kPa)

Overall, the hydroperoxide, acid and water contents are related to each other. The decomposition of an hydroperoxide generates a water and an alcohol molecules. If it is a primary alcohol, it can evolve to a carboxylic acid. The accumulation of one of these compounds is an indicator of the relative rates of the successive reactions. With the mono-aromatic compound, the quantity of peroxide and water are high but the acid number is low. This means that the rates of formation of peroxides and water are higher than their consumptions. In this case, the limiting step is the transformation of the alcohol into the corresponding carboxylic acid. On the contrary, for the 1-MN, the hydroperoxide quantity remains rather low and the quantities of water and acid increase linearly. This means that the rates of formation and consumption of hydroperoxide molecules are equal. In the case of the n-C<sub>12</sub>, the quantity of peroxides and acids increases linearly but the evolution of the quantity of water, which was linear at the beginning, slows down and could reach a plateau at higher  $\Delta P/P_{\max}$ . For the n-C<sub>12</sub> IsoB, the quantity of peroxides reaches a plateau but the evolutions of water and acid remain linear. Finally, for the n-BC, the quantities of hydroperoxides and water stabilize. All these evolutions are very complex and dependent of the nature of the compounds. Simulation would be necessary to understand the behavior of the molecules.

## Kinetic study

A final experimental investigation was dedicated to the determination of degradation kinetic constants by performing tests at  $\Delta P/P_{\max} = 10\%$  with an initial  $O_2$  pressure of 700 kPa but for three temperatures: 140, 150 and 160 °C. The evolution of the pressure as the reaction proceeds for the three temperatures have similar shapes but the maximum pressure reached increases with increasing temperature while the time to reach the targeted  $\Delta P/P_{\max}$  decreases. The IP values obtained (Table 2) confirm the impact of temperature on the induction time. Indeed, the higher the temperature is, the shorter the induction time is. As before, the evolution of the oxidation reaction is followed using the number of moles of reactants consumed. These values are plotted in Figure 10 for all the model molecules and for the three temperatures considered. In general, the consumption of reagents increases with temperature. Moreover, oxygen is always the reagent consumed in majority compared to the hydrocarbon molecules, whatever the temperature is. As a reminder,  $\Delta P/P_{\max}$  is directly related to the consumption of oxygen. Thus, the temperature accelerates the rate of oxygen consumption between 140 and 160 °C, whatever the oxidized molecule is.

Nevertheless, it is not possible to directly compare the induction periods as it has been done in previous works [42-[44]. Indeed, at a fixed  $\Delta P/P_{\max}$ , the quantitative analysis performed in this study highlights that the oxygen conversions are not identical at 140 and 160 °C. Due to the temperature difference, the maximum pressure ( $P_{\max}$ ) obtained in the batch system is not the same. This has an impact on the calculation of the  $\Delta P$  and, consequently, on the level of oxygen consumption. Therefore, to highlight the real impact of temperature, the tests should have been carried out at iso-conversion of oxygen, i.e. at the same oxygen consumption and not at the same  $\Delta P/P_{\max}$ . It was quite easy to estimate the additional time required with the previously calculated oxygen consumption rate, expressed in mmol/s. It should be noted that this assumption was confirmed by performing tests with corrected induction periods and iso-conversion of oxygen in the case of n-C<sub>12</sub> [6]. The corrected induction periods (IP) are present in Table 2 and will be useful for the kinetic study.

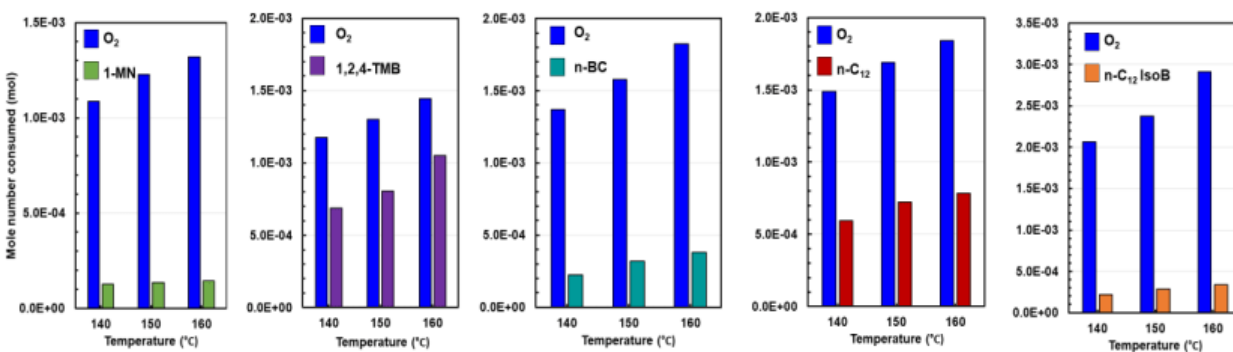


Figure 10 - Evolution as a function of temperature of the number of moles of O<sub>2</sub> and model molecule consumed ( $\Delta P/P_{\max} = 10\%$ ,  $P_{O_2,i} = 700$  kPa)

Table 2 - IP<sub>s</sub> results obtained experimentally for different temperature at  $\Delta P/P_{max} = 10\%$  and after correction ( $P_{O_2,i} = 700$  kPa).

	Temperature (°C)	140	150	160
1-MN	Experimental IP (min)	1379	924	587
	Corrected IP (min)	1676	993	587
1,2,4-TMB	Experimental IP (min)	156	75	39
	Corrected IP (min)	192	83	39
n-BC	Experimental IP (min)	145	58	26
	Corrected IP (min)	193	67	26
n-C <sub>12</sub>	Experimental IP (min)	169	71	33
	Corrected IP (min)	209	78	33
n-C <sub>12</sub> IsoB	Experimental IP (min)	127	59	30
	Corrected IP (min)	180	73	30

### Global reaction rate constant

Based on the same methodology presented in a previous paper [6], it was possible to determine the overall oxidation reaction kinetic constants of the set of model molecules presented in this study. Bacha *et al.* [44] analysis were used to determine the overall reaction rate parameters, without any approximation about the mole fraction consumed during the induction period of the oxygen and fuel data. The global reaction rate parameters for the calculation of the constant  $k$  were determined experimentally and taking into account the corrected experimental induction times (Table 2). Thus, their equation was modified to take into account these new elements as shown in Equation 2 where  $\Delta n(O_2)$  and  $\Delta n(RH)$  the numbers of moles of dioxygen and hydrocarbon molecule consumed respectively,  $IP_{corrected}$  is expressed in seconds.

$$\ln \left[ \frac{\Delta n(O_2)}{\Delta n(RH)IP_{corrected}} \right] = - \frac{E_a}{RT} + \ln A \quad \text{Equation 2}$$

The corrected induction periods (Table 2) were plotted as a function of  $1/T$  on Figure 11. A straight line was obtained by linear regression allowing to determine the values  $E_a$  and  $A$  (Table 3). The back calculated rate constants  $k$  of the oxidation reaction of all model molecules are presented in Table 4 for each test temperature. They were then deduced by using Arrhenius regression estimates. By comparing the kinetic values obtained for all the model molecules, it is possible to distinguish the model compounds into two categories:

- alkanes with high activation energy values ( $E_a > 120$  kJ.mol<sup>-1</sup>) and high pre-exponential factors ( $A \sim 10^{+12}$ );
- aromatics with somewhat lower activation energies ( $E_a < 110$  kJ.mol<sup>-1</sup>) and pre-exponential factors ( $A < 10^{+09}$ ).

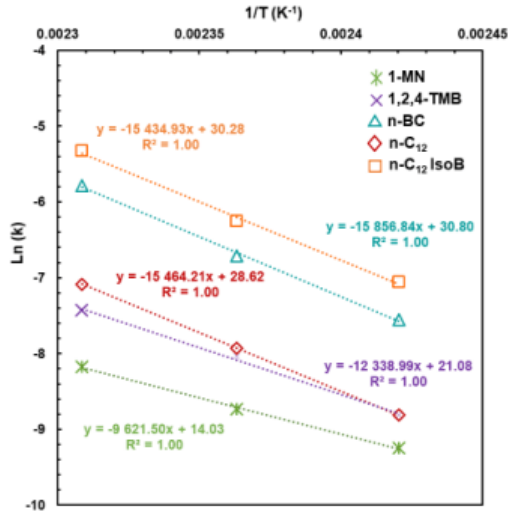


Figure 11 - Experimental model of the kinetics constant of the hydroperoxide dissociation of all the model molecules oxidation ( $\Delta P/P_{max}=10\%$ ,  $P_{O_2,i}=700$  kPa)

Table 3 - Activation energies ( $E_a$ ) and pre-exponential factors  $A$  values obtained for the oxidation reaction of all model molecules ( $\Delta P/P_{max} = 10\%$  et  $T = 140$  à  $160^\circ\text{C}$ )

	$E_a$ (kJ.mol <sup>-1</sup> )	$A$ (s <sup>-1</sup> )
<b>1-MN</b>	80.03	$1.25 \cdot 10^{+06}$
<b>1,2,4-TMB</b>	102.73	$1.48 \cdot 10^{+09}$
<b>n-BC</b>	131.79	$2.36 \cdot 10^{+13}$
<b>n-C<sub>12</sub></b>	128.79	$2.86 \cdot 10^{+12}$
<b>n-C<sub>12</sub> IsoB</b>	128.36	$1.42 \cdot 10^{+13}$

Table 4 - Kinetic constants ( $k$ ) of model molecules oxidation determined using Arrhenius regression estimates from Table 3

Temperature (°C)	140	150	160
<b>1-MN</b>	$9.65 \cdot 10^{-05}$	$1.61 \cdot 10^{-04}$	$2.83 \cdot 10^{-04}$
<b>1,2,4-TMB</b>	$1.49 \cdot 10^{-04}$	$3.24 \cdot 10^{-04}$	$5.91 \cdot 10^{-04}$
<b>n-BC</b>	$5.23 \cdot 10^{-04}$	$1.22 \cdot 10^{-03}$	$3.08 \cdot 10^{-03}$
<b>n-C<sub>12</sub></b>	$1.49 \cdot 10^{-04}$	$3.61 \cdot 10^{-04}$	$8.39 \cdot 10^{-04}$
<b>n-C<sub>12</sub> IsoB</b>	$8.63 \cdot 10^{-04}$	$1.92 \cdot 10^{-03}$	$4.85 \cdot 10^{-03}$

### Hydroperoxide dissociation rate constant

Taking into account the qualitative and quantitative results of the liquid phase of the present study, it can be suggested that the secondary oxidation products (alcohols, ketones, aldehydes and carboxylic acid) are generated from the formation and decomposition of hydroperoxides. Based on this hypothesis, it is possible to establish the evolution of the hydroperoxide concentration as a function of the duration of the oxidation reaction using the peroxide values determined experimentally for each temperature. By using the same methodology as in the kinetic study of n-C<sub>12</sub> [6], it is possible to determine the kinetic constant of the hydroperoxide dissociation ( $k''$ ) obtained for each temperature tested Table 6 and from the formalism of the Arrhenius law it was possible to plot  $\ln(k'')$  as a function of  $1/T$  as illustrated in Figure 12.

By comparing the values of the global constant  $k$  (Table 4) and the dissociation of the hydroperoxides constant  $k''$  (Table 6) it can be seen that  $k$  is lower than  $k''$ . This result indicates that the hydroperoxides are consumed very fast after their formation and confirms the experimental results obtained in this study.

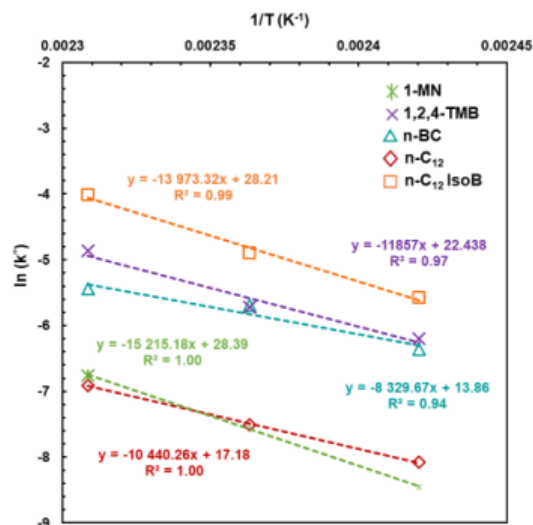


Figure 12 - Experimental model of the propagation kinetic constants of the hydroperoxide dissociation ( $k''$ ) for all the model molecules oxidation ( $\Delta P/P_{max}=10\%$ ,  $P_{O_2,i}=700$  kPa)

Table 5- Activation energies ( $E_a''$ ) and pre-exponential factors  $A''$  values obtained for the hydroperoxide dissociation oxidation reaction for all model molecules ( $\Delta P/P_{max} = 10\%$  and  $T = 140$  to  $160$  °C)

	$E_a''$ (kJ.mol <sup>-1</sup> )	$A''$ (s <sup>-1</sup> )
<b>1-MN</b>	126.50	$2.14 \cdot 10^{+12}$
<b>1,2,4-TMB</b>	98.58	$5.56 \cdot 10^{+09}$
<b>n-BC</b>	69.25	$1.05 \cdot 10^{+06}$
<b>n-C<sub>12</sub></b>	86.80	$2.89 \cdot 10^{+07}$
<b>n-C<sub>12</sub> IsoB</b>	116.17	$1.78 \cdot 10^{+12}$

Table 6 - Kinetic constants ( $k''$ ) of the hydroperoxide dissociation during model molecules oxidation determined using Arrhenius regression estimates from Table 5 and the experimental peroxide values (PV)

Temperature (°C)	140	150	160
<b>1-MN</b>	$2.12 \cdot 10^{-04}$	$5.34 \cdot 10^{-04}$	$1.16 \cdot 10^{-03}$
<b>1,2,4-TMB</b>	$2.04 \cdot 10^{-03}$	$3.29 \cdot 10^{-03}$	$7.70 \cdot 10^{-03}$
<b>n-BC</b>	$1.72 \cdot 10^{-03}$	$3.36 \cdot 10^{-03}$	$4.35 \cdot 10^{-03}$
<b>n-C<sub>12</sub></b>	$3.10 \cdot 10^{-04}$	$5.50 \cdot 10^{-04}$	$9.96 \cdot 10^{-04}$
<b>n-C<sub>12</sub> IsoB</b>	$3.79 \cdot 10^{-03}$	$7.48 \cdot 10^{-03}$	$1.81 \cdot 10^{-02}$

## CONCLUSION

This study proposes a robust procedure for the study of the autoxidation mechanism of model molecules alkanes and mono- and di-aromatics using the PetroOXY device. A complete characterization of all products formed at low progress values ( $\Delta P/P_{max} = 2-10\%$ ) with a fixed temperature and initial oxygen pressure ( $T = 160$  °C and  $P_{O_2} = 700$  kPa) was presented. The individual oxidation of the model molecules highlighted that the "structure-reactivity" relationship is very important in the autoxidation process as attested by different experimental results.

The first is the consumption of oxygen, which is higher than that of the parent hydrocarbons. This high oxygen consumption suggests that oxygen is used in two types of competitive reactions: with the parent hydrocarbon and with the oxidation products. Although the overall behavior of oxygen consumption is similar for all alkane molecules; for aromatics the behavior varies according to their structure. This first aspect is important because it clearly shows a difference in behavior depending on the nature and structure of the oxidized molecules. This difference in behavior is linked directly to the sensitivity of the hydrocarbons to oxidation. This was illustrated in particular by the induction periods. It was observed that the degree of branching of a molecule had an impact on its reactivity: the more branches there are, the shorter is the induction period.

The structure-reactivity aspect was also highlighted through the successive characterization of the gas and liquid phases, which allowed to identify and quantify the oxidation products. In the gas phase, the quantities of the gas products generated are very small. However, these are identical regardless of the nature of the model molecule.

In addition, the liquid phase analyses revealed several classes of oxidation products depending on the initial structure of the model molecules: (i) hydroperoxides from the first oxidation step; (ii) oxidized products with a carbon chain equal to the initial molecule ; (iii) a supplementary class of molecules has been highlighted only in the case of alkanes, products with a shorter carbon chain, resulting from the breaking of the carbon chain of the model molecules. The presence of this third class of molecule probably depends on the degree of branching present on the initial hydrocarbons.

As the PetroOXY apparatus is a closed system, the temperature has a direct impact on the pressure and therefore on the induction period. Using the measured oxygen consumption rate, it was possible to correct the IP values which were then used for the kinetic calculations. Therefore, the overall kinetic constant of the oxidation reaction was calculated with a modified equation taking into account all experimental parameters, *i.e.* the mole fraction of oxygen consumption and the initial hydrocarbons with corrected induction period. In addition, a calculation was also proposed for the dissociation rate of hydroperoxides.

To better understand the degradation of a jet fuel, the next step is to blend all the families of molecules studied individually in this study, in the proportions of a Jet A-1 to approximate a surrogate. Thus, by using the same approach and associating other characterization techniques, such as GCxGC, it would be possible to determine the kinetic parameters capable of calibrating the numerical simulation models of deposits formation.

## REFERENCES

- [1] Heneghan S. P., Zabarnick S., Oxidation of jet fuels and the formation of Deposits, *Fuel*, 1994, 73, 1, 35-43.
- [2] Kuprowicz N. J., Ervin J.S., Zabarnick S., Modeling the liquid-phase oxidation of hydrocarbons over a range of temperatures and dissolved oxygen concentrations with pseudo-detailed chemical kinetics, *Fuel*, 2004, 83 1795– 1801.
- [3] Jalan A, Alecu IM, Meana-Pañeda R, Aguilera-Iparraguirre J, Yang KR, Merchant SS, et al. New pathways for formation of acids and carbonyl products in low- temperature oxidation: the korcek decomposition of  $\gamma$ -ketohydroperoxides. *J. Am. Chem. Soc.* 2013;135(30):11100–14.
- [4] Marteau C, Ruyffelaere F, Aubry J-M, Penverne C, Favier D, Nardello-Rataj V. Oxidative degradation of fragrant aldehydes, Autoxidation by molecular oxygen. *Tetrahedron*, 2013,69 (10),2268–75.
- [5] Webster, R.L., Rawson, P.M., Kulsing, C., Evans, D.J., Marriott, P.J., Investigation of the thermal oxidation of conventional and alternate aviation fuels with comprehensive two-dimensional gas chromatography accurate mass quadrupole time-of-flight mass spectrometry, *Energy Fuels*, 2017, 31, 4886–4894.
- [6] Aminane S., Sicard M., Melliti Y., Ser F., Lorette Sicard L., Experimental study of the kinetics of degradation of n-dodecane under thermo-oxidative stress at low temperature and mechanism inferred, *Fuel*, 2021, 307,121669.
- [7] Christison, K.M., Lorenz, R.M., Xue, L., Sparkman, O.D., Exploring the molecular origin of jet fuel thermal oxidative instability through statistical analysis of mass spectral data, *Energy Fuels*, 2019, 33, 830–836.

- [8] Kabana, C.G., Botha, S., Schmucker, C., Woolard, C., Beaver, B., Oxidative stability of middle distillate fuels. Part 1: exploring the soluble macromolecular oxidatively reactive species (SMORS) mechanism with jet fuels, *Energy Fuels*, 2011, 25,(11) 5145–5157.
- [9] Beaver, B., Gao, L., Burgess-Clifford, C., Sobkowiak, M., On the mechanisms of formation of thermal oxidative deposits in jet fuels. Are unified mechanisms possible for both storage and thermal oxidative deposit formation for middle distillate fuels, *Energy Fuels*, 2005, 19, 1574–1579.
- [10] Commodo, M., Fabris, I., Wong, O., Groth, C.P.T., Gülder, Ö.L., Threedimensional fluorescence spectra of thermally stressed commercial Jet A-1 aviation fuel in the autoxidative regime, *Energy Fuels*, 2012, 26, 2191–2197.
- [11] Aksoy, P., Gül, Ö., Cetiner, R., Fonseca, D.A., Sobkowiak, M., Falcone-Miller, S., Miller, B.G., Beaver, B., Insight into the mechanisms of middle distillate fuel oxidative degradation. Part 2: on the relationship between jet fuel thermal oxidative deposit, soluble macromolecular oxidatively reactive species, and smoke point, *Energy Fuels*, 2009, 23, 2047–2051.
- [12] Jia, T., Pan, L., Gong, S., Xie, J., Wang, X., Fang, Y., Zou, J.-J., Zhang, X., Mechanistic insights into the thermal deposition of highly thermal-stable jet fuel, *Fuel*, 2020, 276, 118100.
- [13] Venkataraman, R., Eser, S., Characterization of solid deposits formed from short durations of jet fuel degradation: carbonaceous solids. *Ind. Eng. Chem. Res.*, 2008, 47, 9337–9350.
- [14] Jones E. G., Balster W.J., Phenomenological Study of the Formation of Insolubles in a Jet-A Fuel, *Energy & Fuels* 1993, 7, 968-977.
- [15] Chatelain K., Nicolle A., Ben Amara A., Catoire L., Starck L., Wide Range Experimental and Kinetic Modeling Study of Chain Length Impact on n-Alkanes Autoxidation, *Energy Fuels*, 2016, 30, 1294–1303.
- [16] Edwards, T., Cracking and deposition behavior of supercritical hydrocarbon aviation fuels, *Combust. Sci. Technol.*, 2006, 178, 307–334.
- [17] Tao Z., Fu Y., Xu G., Deng H., Jia Z., Experimental study on influences of physical factors to supercritical RP-3 surface and liquid-space thermal oxidation coking, *Energy Fuels*, 2014, 28, 6098–6106.
- [18] Kuprowicz, N. J., Zabarnick, S. West, Z. J., Ervin J. S. Use of Measured Species Class Concentrations with Chemical Kinetic Modeling for the Prediction of Autoxidation and Deposition of Jet Fuels, *Energy & Fuels* 2007, 21, 530-544.
- [19] Velkavrh, I., Palamarciuc, I., Galus D.G., Diem, A., Brenner, J., Gabler, C., Mellor, B., Ratoi, M., Formation of surface deposits on steel and titanium aviation fuel tubes under real operating conditions. *ACS Omega*, 2019, 4, 8255–8273.
- [20] Fu, Y., Xu, G., Wen, J., Huang, H., Thermal oxidation coking of aviation kerosene RP-3 at supercritical pressure in helical tubes, *Appl. Therm. Eng.* 2018, 128, 1186–1195.
- [21] Jiang, H., Ervin, J.S., Zabarnick, S., West, Z., Effects of flow passage expansion or contraction on jet-fuel surface deposition. *J. Propuls. Power*, 2012, 28, 694–706.
- [22] Han Z., Zhou W., Zan H., Jia Z., Martynenko S., Yanovskiy L., Numerical investigation on influences of inlet flow pattern on RP-3 thermal oxidation deposition, *Fuel*, 2021, 303, 121314.
- [23] Sander Z.H., West Z.J., Ervin J.S., Zabarnick S., Experimental and Modeling Studies of Heat Transfer, Fluid Dynamics, and Autoxidation Chemistry in the Jet Fuel Thermal Oxidation Tester (JFTOT), *Energy Fuels*, 2015, 29, 7036-7047.
- [24] Pei X-Y, Hou L-Y., Effect of dissolved oxygen concentration on coke deposition of kerosene, *Fuel Processing Technology*, 2016, 142, 86–91.
- [25] Adams, R.K., Zabarnick, S., West, Z.J., Striebich, R.C., Johnson, D.W., Chemical analysis of jet fuel polar, heteroatomic species via high-performance liquid chromatography with electrospray ionization–mass spectrometric detection, *Energy Fuels*, 2013, 27, 2390–2398.
- [26] Zabarnick, S., West, Z.J., Shafer, L.M., Mueller, S.S., Striebich, R.C., Wrzesinski, P.J., Studies of the role of heteroatomic species in jet fuel thermal stability: model fuel mixtures and real fuels, *Energy Fuels*, 2019, 33, 8557–8565.

- [27] Sobkowiak, M., Griffith, J.M., Wang, B., Beaver, B., Insight into the mechanisms of middle distillate fuel oxidative degradation. Part 1: on the role of phenol, indole, and carbazole derivatives in the thermal oxidative stability of Fischer-Tropsch/petroleum jet fuel blends, *Energy Fuels*, 2009, 23, 2041–2046.
- [28] Rawson, P.M., Webster, R.L., Evans, D., Abanteriba, S., Contribution of sulfur compounds to deposit formation in jet fuels at 140 °C using a quartz crystal microbalance technique, *Fuel*, 2018, 231, 1–7.
- [29] AlGhani, M.J.A., Comparative study in evaluating the antioxidation efficiency for native type's antioxidants extracted from crude oil with the synthesized class, *World Acad. Sci. Eng. Technol.*, 2016, 10, 1345–1348.
- [30] Waynick, J.A., The development and use of metal deactivators in the petroleum industry: a review, *Energy Fuels*, 2001, 15, 1325–1340.
- [31] West, Z.J., Adams, R.K., Zabarnick, S., Homogeneous catalysis of liquid-phase hydroperoxide decomposition in hydrocarbons, *Energy Fuels*, 2011, 25, 897–904.
- [32] Antonio, E.N., Wicking, C., Filip, S., Ryan, M.P., Heutz, S., Role of iron speciation in oxidation and deposition at the hexadecane-iron interface, *ACS Appl. Mater. Interfaces*. 2020, 12, 19140–19152.
- [33] Pfaendtner J., Broadbelt L.J., Elucidation of structure–reactivity relationships in hindered phenols via quantum chemistry and transition state theory, *Chemical Engineering Science*, 2007, 62, 5232 - 5239.
- [34] ASTM D7545 - 09 Standard Test Method for Oxidation Stability of Middle Distillate Fuels—Rapid Small Scale Oxidation Test (RSSOT), ASTM International: West Conshohocken, PA, 2009.
- [35] West ZJ, Zabarnick S, Striebich RC. Determination of hydroperoxides in jet fuel via reaction with triphenylphosphine. *Ind. Eng. Chem. Res.* 2005;44(10):3377–83.
- [36] Wiklund P, Karlsson C, Levin M. Determination of hydroperoxide content in complex hydrocarbon mixtures by gas chromatography/mass spectrometry. *Anal Sci* 2009;25(3):431–6.
- [37] ASTM D 3703-13 - Standard Test Method for Hydroperoxide Number of Aviation Turbine Fuels, Gasoline and Diesel Fuels, ASTM International: West Conshohocken, PA, 2013.
- [38] Pullen J, Saeed K. An overview of biodiesel oxidation stability. *Renew Sustain Energy Rev* 2012;16 (8),5924–50.
- [39] ASTM D3242-08 - Standard Test Method for Acidity in Aviation Turbine Fuel., ASTM International: West Conshohocken, PA, 2008.
- [40] Blin-Simiand N., Jorand F., Sahetchian K., Hydroperoxides With Zero, One, Two or More Carbonyl Groups Formed During the Oxidation of N-Dodecane, *Combustion and Flame*, 2001, 126, 1524–1532.
- [41] Sarathy SM, Westbrook CK, Mehl M, Pitz WJ, Togbe C, Dagaut P, et al. Comprehensive chemical kinetic modeling of the oxidation of 2-methylalkanes from C7 to C20. *Combust Flame* 2011;158(12):2338–57.
- [42] Ben Amara A, Nicolle A, Alves-Fortunato M, Jeuland N. Toward predictive modeling of petroleum and biobased fuel stability: kinetics of methyl oleate/n-dodecane autoxidation. *Energy Fuels* 2013;27(10):6125–33.
- [43] Chatelain K, Nicolle A, Ben Amara A, Starck L, Catoire L. Structure–reactivity relationships in fuel stability: experimental and kinetic modeling study of isoparaffin autoxidation. *Energy Fuels* 2018;32(9):9415–26.
- [44] Bacha K, Ben-Amara A, Vannier A, Alves-Fortunato M, Nardin M. Oxidation stability of diesel/biodiesel fuels measured by a petrooxy device and characterization of oxidation products. *Energy Fuels* 2015;29(7):4345–55.